Polarization dependent near-field speckle of random gold films

Julien Laverdant,[*] Stéphanie Buil, Bruno Bérini, and Xavier Quélin

Groupe d'Etude de la Matière Condensée (UMR 8635), Université de Versailles-Saint-Quentin-en-Yvelines, 45, Avenue des Etats-Unis, 78035 Versailles, France

The near-field speckle of random gold nanostructures is experimentally and theoretically investigated. The topography and the intensity distribution, under polarized illumination, are obtained with an aperture scanning near-field optical microscope. The sharpness of the experimental images entitles us to perform a fine statistical analysis based on the autocorrelation function (ACF). The intensity ACF clearly exhibits an anisotropic behavior and subwavelength oscillations, depending on the incident polarization. A comparison with a numerical simulation exhibits the influence of the surface topography on the anisotropic near-field speckle.

PACS number(s): 07.79.Fc, 61.43.Hv, 42.25.Dd

I. INTRODUCTION

The problem of light scattering through randomly inhomogeneous medium has been extensively studied (see, for example, Refs. [1–3]), and it is well known that the resulting intensity distribution is a complex interference pattern, known as speckle. This intensity pattern displays highly irregular fluctuations which are due to the specific properties of the studied medium. It has been clearly established that the appearance of the speckle pattern is due to the short range correlations of the wave transmitted or reflected by the random medium.[4–7] To exhibit these behaviors, one of the most relevant statistical analyses is the autocorrelation function (ACF) which is a second-order statistical function giving information on the measured signal fluctuations.[8] In the far field, the spatial correlation of the speckle usually exhibits a circular symmetry whereas the contribution of evanescent waves changes the appearance of the near-field speckle.

One of the earliest theoretical studies of near-field speckle pattern by using the intensity ACF[9] predicted the relationship between the scattered intensity cross-correlation and the statistical properties of the rough scattering surface. The existence of short range correlations was verified by Emiliani *et al.*[10] in near-field experiments performed in dielectric medium. The transition between near-field and far-field speckle patterns[11] has been observed in the intensity correlations from random dielectric media. It was also observed that the contribution of evanescent waves modifies the speckle in the near field: subwavelength correlations and a strong distance-to-surface dependence have been pointed out. More recently, it has been numerically predicted that the near-field speckle of rough interface exhibits an anisotropic figure which is due to the polarization-dependent coupling between the evanescent waves.[12]

In this paper, we propose the experimental evidence of this coupling. Experimental and theoretical results are presented on random gold thin films. The near-field experimental results have been obtained with an aperture scanning near-field optical microscope (SNOM) in collection mode. The setup allows us to control the incident polarization and the quality of the optical images is good enough to exhibit the anisotropy of the near-field speckle and its polarization dependence. Based on the model proposed in Ref. [9], numeri-

cal simulations taking account of the real topographic distribution support the experimental results.

In Sec. II, the metallic samples under study are presented and characterized by atomic force microscopy (AFM) and spectrophotometry. The ACF of the topographic distribution is studied to deduce the surface correlation length.[13,14] Then, in Sec. III, near-field optical results are presented with the corresponding intensity ACF. The influence of the incident polarization on surface scattering is analyzed. In Sec. IV, numerical simulations[9] are presented to be compared to the experimental results and the influence of the topographic distribution is discussed. A summary is given in Sec. V.

II. TOPOGRAPHIC AND FAR-FIELD OPTICAL PROPERTIES OF A GOLD FILM NEAR THE PERCOLATION THRESHOLD

Samples were prepared by thermal evaporation on a glass quartz substrate at room temperature and under ultrahigh vacuum (10^{-9} torr). The deposited thin films appear as composite media with metallic nanosized particles and present very specific optical properties depending on the metallic-surface coverage. For example, the well-known surface plasmon resonances[15] can result in fluctuations of the electromagnetic energy near the surface. These fluctuations are more emphasized at the vicinity of the metallic concentration leading to the insulator-conductor transition, identified as the percolation threshold.[16] In Fig. 1, spectrophotometric results of the sample near this threshold are presented. Due to surface plasmon resonances for near-percolated gold films, the absorption graph presents a well-known large flat plateau[17] nearly independent of the wavelength in the red to midinfrared range of the spectrum. The absorbance minimum near 510 nm can then be considered as out of surface plasmon resonances. Only surface scattering is expected near this wavelength.

AFM (Veeco Dimension 3100) scans in tapping mode are performed to determine the height distributions $S(x,y)$, where (x,y) are the Cartesian coordinates of the images. In Fig. 2, we present a typical AFM image ($1 \times 1 \ \mu m^2$, 512×512 points) of the near-percolated sample under study. Interconnected clusters which are a fingerprint of near-percolated gold film structure are clearly observed on the
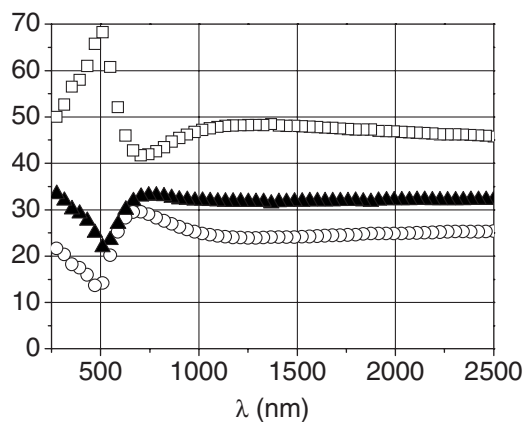
FIG. 1. Spectrophotometric measurements of a semicontinuous gold film near the percolation threshold (the metallic surface coverage is 59%): ($\square$) transmission, ($\blacktriangle$) absorption and ($\bigcirc$) Reflection spectra.

FIG. 2. (Color online) AFM map, obtained in tapping mode, of a semicontinuous gold film. The metallic surface coverage is 59%.

AFM image. The mean roughness σ is defined by

$$\sigma^2 = \langle S^2(x,y) \rangle - \langle S(x,y) \rangle^2. \tag{1}$$

For the sample presented in Fig. 2, the roughness is $\sigma \simeq 2$ nm which is a mean value for different samples at the same metallic coverage. From this surface profile, we calculate the surface ACF. The normalized surface ACF is defined as

$$g(u,v) = \frac{\langle S(x,y)S(x+u,y+v) \rangle}{\langle S(x,y) \rangle \langle S(x+u,y+v) \rangle}, \tag{2}$$

where $\langle \, \rangle$ denotes the spatial average over the (x,y) coordinates of the AFM data. The calculated surface ACF is presented in Fig. 3(a).

The $g(u,v)$ function in Fig. 3(a) is clearly isotropic which is in good agreement with an isotropic growth process. Then, the correlation function is averaged at constant distance as

$$C_S(R) = \langle g(u,v) - 1 \rangle_R, \tag{3}$$

where $R^2 = u^2 + v^2$. $C_S(R)$, normalized by its value at $R=0$, is plotted in Fig. 3(b) and is quite well adjusted by a Gaussian function which allows us to define the correlation length ξ.[13] This correlation length is the average distance between two points of the same cluster and is found equal to $\xi = 15$ nm.

This value and this topographic analysis will be used further in Sec. IV A to simulate the optical ACF.

III. NEAR-FIELD EXPERIMENTAL RESULTS

Experiments were performed with a commercial near-field optical microscope (Veeco, Aurora 2). The SNOM probe is an Al-coated optical fiber tip with a 50 nm aperture which is mounted on a quartz tuning fork.[18] The tip-to-sample distance is regulated by shear force detection. An Ar/Kr laser is used to illuminate the sample under normal incidence. The laser is transmitted through the sample and the scattered light is collected through the fiber tip. The laser line used is $\lambda = 514.5$ nm with an incident power of 10 mW and the incident polarization is linear and is adjusted by a Fresnel rhomb retarder.

In Fig. 4, we present typical, 5×5 μm^2 with 400×400 data points, topographic [Fig. 4(a)] and optical [Fig. 4(b)] images obtained on a gold film near the percolation threshold. Deduced from these intensity data points, the intensity histogram, which is called probability distribution function (PDF), is also displayed [Fig. 4(c)].

The optical image displays low intensity variations and is the negative of the topographic image. The PDF displays a
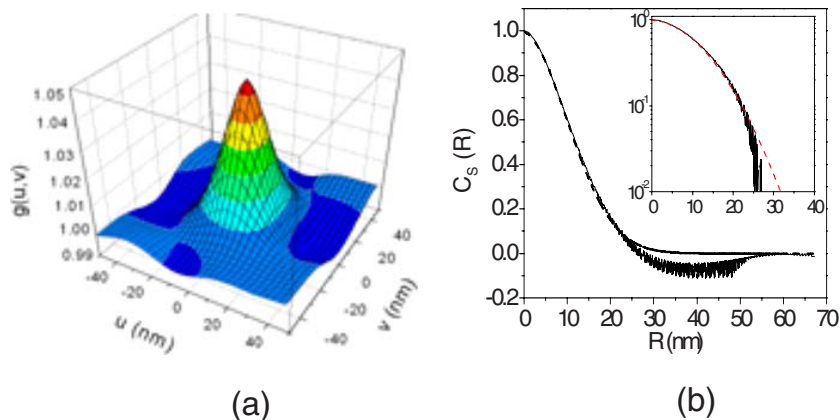
FIG. 3. (Color online) (a) Autocorrelation function of the surface profile for a granular gold film. (b) The polar correlation curve $C_S(R)$ fitted by a Gaussian-like function (dashed line).
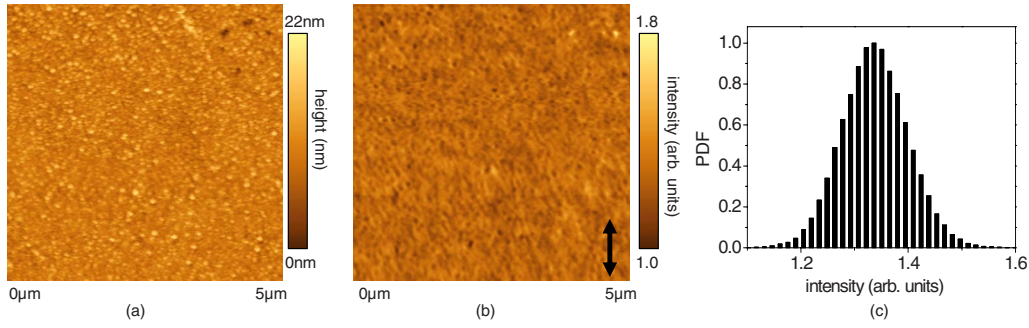
FIG. 4. (Color online) (a) Topographic image of a gold film near the percolation threshold. (b) SNOM image at $\lambda=514.5$ nm (400 $\times$400 data points, the incident linear polarization is indicated by the arrow). (c) Corresponding probability density function (PDF).

narrow symmetric distribution centered on 1.35 which is in good agreement with the statistical behavior expected for an out of plasmon resonance regime.[19]

The intensity autocorrelation function $C_I(\Delta x, \Delta y)$ is calculated with the same procedure used for the AFM measurements and is presented in Fig. 5. We observe that the central peak in Fig. 5(a) is stretched in the direction of the incident field polarization (Δy). Moreover, subwavelength oscillations of pseudoperiod $\sim$160 nm are clearly observed in the perpendicular direction (Δx). For more clarity, the correlation functions for the two directions, normalized by the value $C_I(0,0)$, $C_I(\Delta x,0)$ (perpendicular to the direction of incident field) and $C_I(0,\Delta y)$ (in the parallel direction), have been plotted in Figs. 5(b) and 5(c), respectively. Corresponding to the half width at half maximum (HWHM) of the correlation function, two correlation lengths ξ_x and ξ_y can be defined and we found $\xi_x=33$ nm and $\xi_y=50$ nm. Experiments performed by rotating the incident polarization of 90° clearly show that the intensity autocorrelation map also rotates with the same angle as the polarization.

This near-field anisotropy, completely missing in far-field observations,[7] has been predicted by simulations.[12] It can be attributed to the coupling between evanescent waves from different surface diffusers. This coupling is stronger in the incident polarization direction (Δy), leading to a larger correlation length in this direction. In the transverse direction (Δx), the intensity correlation length is shorter because of stronger scattering. This behavior clearly shows that unlike the far field and due to evanescent wave coupling, the near-field speckle strongly depends on the incident field polarization. A simulation based on the model developed by Greffet and Carminati[9] has been computed to be compared to our experimental results.

IV. NUMERICAL RESULTS

In this section, we present the intensity ACF simulated for our near-percolated gold samples, according to the model previously proposed by Greffet and Carminati.[9] Two different approaches, both based on this model, are used. In the first one, the scattered field distribution is calculated by using the experimental surface profile and the intensity ACF is deduced. In the second approach, the intensity ACF is directly calculated assuming an approximated surface ACF, justified by the Gaussian-like fitting previously adjusted on experimental AFM data (Sec. II).

A. Simulated intensity autocorrelation function using a perturbative model

By using a perturbative method, Greffet and Carminati have calculated the near-field scattering of light by a random
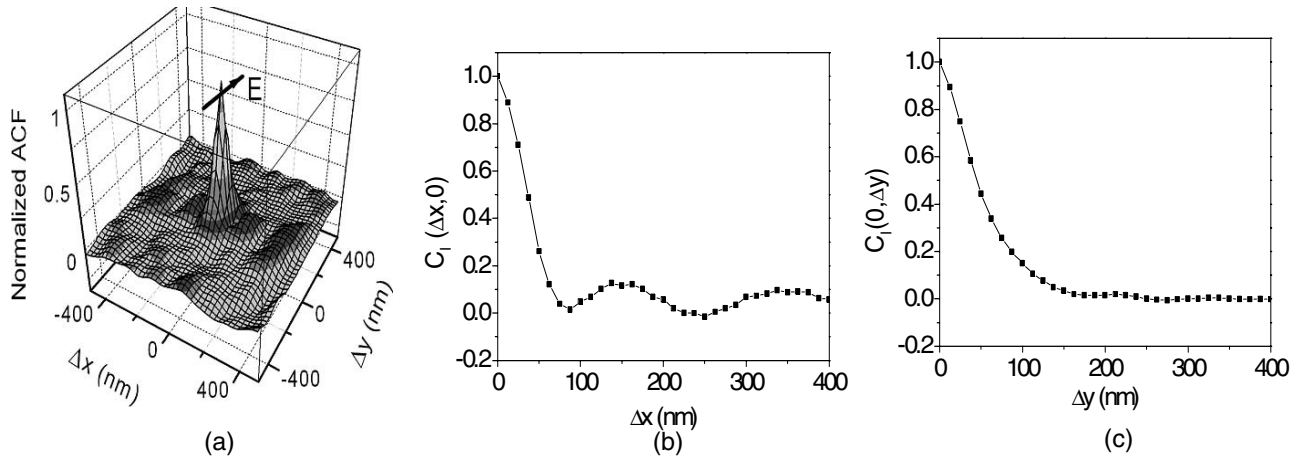
FIG. 5. (a) Three-dimensional mapping of the near-field normalized intensity ACF calculated from SNOM data. The direction of the incident polarization is indicated by an arrow. [(b) and (c)] Correlation curves $C_I(\Delta x,0)$ and $C_I(0,\Delta y)$, respectively.
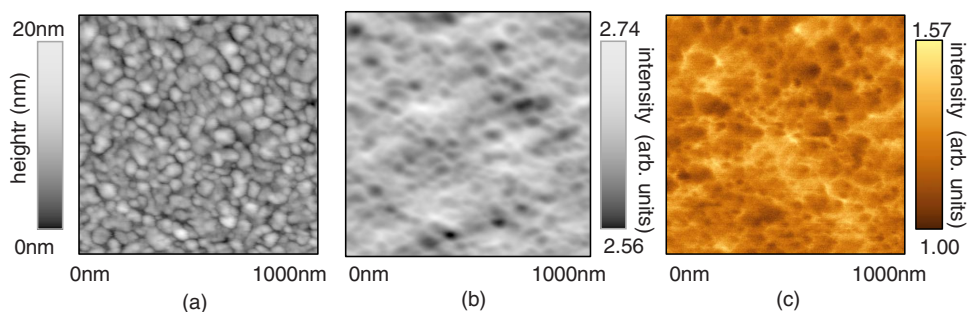
FIG. 6. (Color online) (a) Near-field topographic image of a semicontinuous gold film obtained by SNOM and corresponding optical images: (b) simulated image and (c) experimental intensity distribution.

rough surface.[9] In their article, these authors defined a correlation function of the near-field intensity and demonstrated the direct relationship between the ACF of the intensity and the surface ACF. In order to compare to the experimental results obtained in the previous section, the intensity ACF will be, first, calculated by using the measured surface profile and, second, by using an approximated surface ACF.

The scattered intensity distribution is simulated by using a perturbative approach which has been proved to be valid for randomly rough surfaces with a small enough rms height σ, i.e., $\sigma/\lambda < 5\%$. This condition is completely fulfilled in our case where $\sigma \simeq 2$ nm and $\lambda = 514.5$ nm.

We consider an incident field $\mathbf{e}_{inc}$ coming from the lower half-space $[z < S(x,y)]$, and the theoretical expression of the scattered field $\mathbf{E}(\mathbf{r}_\parallel, z)$ at a distance z from the sample surface in the upper half-space $[z > S(x,y)]$ is given by

$$\mathbf{E}(\mathbf{r}_\parallel, z) = T\mathbf{e}_{inc} + \frac{k_0^2}{4\pi^2}(\varepsilon - 1)T$$

$$\times \int \overset{\leftrightarrow}{G}(\mathbf{k}_\parallel)\mathbf{e}_{inc}\widetilde{S}(\mathbf{k}_\parallel)e^{i\gamma_1(\mathbf{k}_\parallel)z}\exp(i\mathbf{k}_\parallel \cdot \mathbf{r}_\parallel)d\mathbf{k}_\parallel, \quad (4)$$

where $\mathbf{r}_\parallel = (\Delta x, \Delta y)$ is an in-sample-plane vector, T is the Fresnel transmission coefficient, ε is the dielectric constant of the sample, k_0 is the incident wave vector modulus, and $\gamma_1(\mathbf{k}_\parallel) = [k_0^2 - |\mathbf{k}_\parallel|^2]^{1/2}$ with the determination $\mathrm{Re}\{\gamma_1(\mathbf{k}_\parallel)\} > 0$ and $\mathrm{Im}\{\gamma_1(\mathbf{k}_\parallel)\} > 0$. $\widetilde{S}(\mathbf{k}_\parallel)$ is the Fourier component of the surface profile $S(x,y)$. The term $\overset{\leftrightarrow}{G}(\mathbf{k}_\parallel)$ is the Fourier transform of the interface Green's function and is explicitly given in Refs. [20] and [21].

It has been previously demonstrated[12] that the observation distance z plays the same role as a filter for the variations of the intensity ACF. So in order to exhibit mainly the near-field properties of the intensity ACF, an observation distance $z = 1$ nm will be used. In a first approach, $\widetilde{S}(\mathbf{k}_\parallel)$ is deduced from the surface profile measured by SNOM.

In Fig. 6(b), a typical result of the intensity simulated by using Eq. (4) is displayed, with $z = 1$ nm, a linear incident polarization, a dielectric constant of $\varepsilon = -2.5 + 3.26i$ at $\lambda = 514$ nm for a gold thin film,[15] and the measured topography $S(x,y)$ is presented in Fig. 6(a). For the record, the experimental local-field intensity distribution is also shown in Fig. 6(c).

The simulated near-field scattered intensity is of opposite contrast to the measured topography of the metallic thin film as experimentally observed. The surface roughness is low ($\sigma \sim 2$ nm) so that the numerical intensity variations are very weak. From this simulated intensity distribution, we calculate the optical intensity ACF which is presented in Fig. 7.

In Fig. 7(a), one can notice the same anisotropic behavior as previously experimentally observed. The optical intensity is wider in the direction parallel to the incident field. Moreover, the ACF calculated from the simulated intensity distribution exhibits the oscillations observed in Fig. 5(a). The correlation lengths of the simulated near-field intensity in Fig. 7(b), measured as the HWHM, are found to be $\xi'_y = 80$ nm and $\xi'_x = 30$ nm in the Δy and Δx directions, respectively. The anisotropic ratio $\kappa' = \xi'_y/\xi'_x = 2.4$ is quite larger than the experimental one (~ 1.5). The oscillations exhibit a pseudoperiod of nearly 100 nm which is a little bit less than the experimental value of 160 nm deduced from Fig. 5(b). Nevertheless, we can note that the experimental and the numerical values of the correlation lengths and the pseudope-
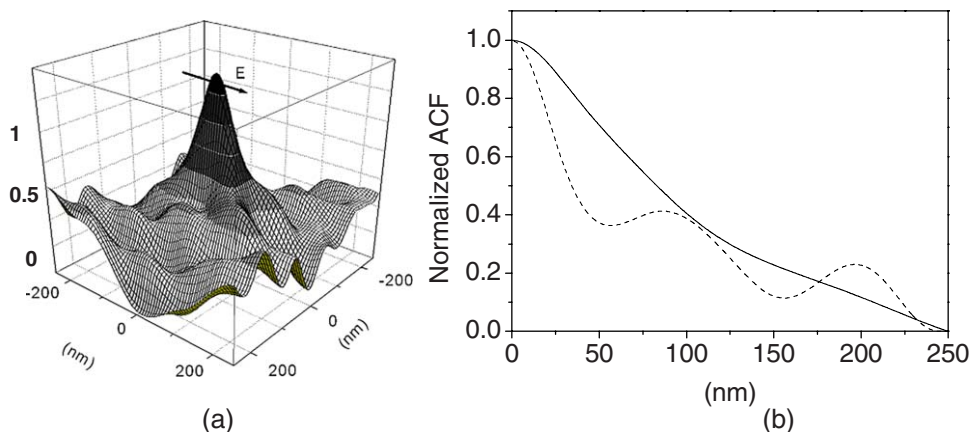
FIG. 7. (Color online) (a) Normalized intensity ACF calculated from the simulated intensity distribution of (b). The incident field is shown by an arrow. (b) one-dimensional (1D) curves plotted in the parallel (solid line) and in the perpendicular (dashed line) directions of the incident field.

(a)

(b)
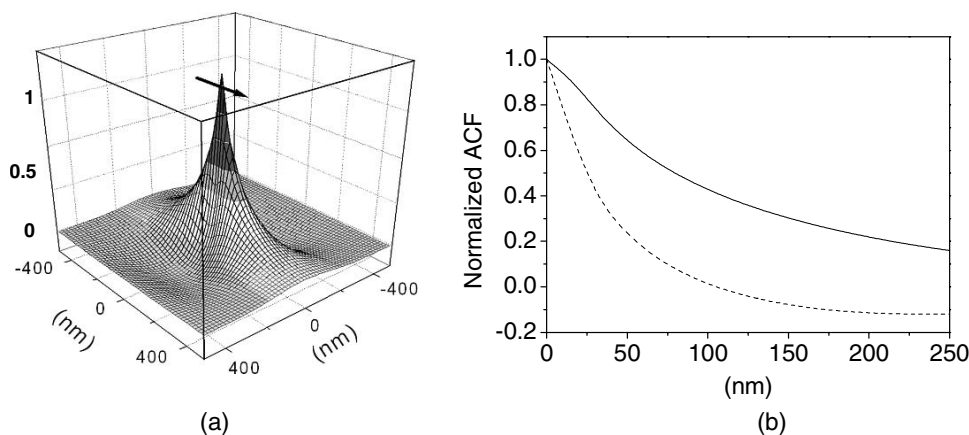
FIG. 8. (a) Near-field intensity ACF simulated with a Gaussian correlated surface. The incident field polarization is indicated by an arrow. (b) The 1D curves are plotted in the parallel (solid line) and in the perpendicular (dashed line) directions of the incident field.

riod of the oscillations are of the same order of magnitude.

To understand the origin of these anisotropic behaviors, several authors used an approximated surface ACF. From the same perturbative model, the spectrum of the correlation function of the near-field intensity is deduced from Eq. (4) and is directly related to the spectral power density of the surface.[9] The analytical expression we use to calculate the intensity ACF $\Gamma_I(\mathbf{r}_\parallel, z)$ is

$$\Gamma_I(\mathbf{r}_\parallel, z) = \int H(\mathbf{k}_\parallel, z)\widetilde{\Gamma}_S(\mathbf{k}_\parallel)\exp(i\mathbf{k}_\parallel \cdot \mathbf{r}_\parallel)d\mathbf{k}_\parallel, \quad (5)$$

where z is the distance between the observation plane and the sample plane and $\widetilde{\Gamma}_S(\mathbf{k}_\parallel)$ is the Fourier transform of the surface autocorrelation function. $H(\mathbf{k}_\parallel, z)$ is a filter given in Refs. 9 and 21 depending on the incident polarization, on the height of the observation point, and on the wave vector of the incident field. In Sec. II, we have adjusted the ACF of the measured surface profile with a Gaussian function that we use now to calculate the intensity ACF.

In order to determine the expression of the filter $H(\mathbf{k}_\parallel, z)$, we use the same dielectric constant of $\varepsilon = -2.5 + 3.26i$ at $\lambda = 514$ nm for a gold thin film [15] and the incident wave polarization is assumed to be linear. The observation distance is set to $z = 1$ nm, in order to compare with the first approach. The resulting map of the intensity ACF $C_I(\mathbf{r}_\parallel, z=1)$ is presented in Fig. 8(a).

The optical intensity ACF is wider in the direction parallel to the incident field as previously numerically and experimentally observed. Deduced from these simulations, the correlation lengths are found to be $\xi''_y = 80$ nm and $\xi''_x = 33$ nm in the Δy (parallel to the incident field polarization) and Δx

directions, respectively. Furthermore, we note that the fluctuating part of the intensity ACF, experimentally observed in the x direction (perpendicular to the incident field polarization), is not retrieved. The anisotropic ratio $\kappa'' = \xi''_y / \xi''_x = 2.6$ obtained with this simulation is comparable to the value $\kappa' = 2.4$ obtained with the first approach.

By using an approximate surface profile spectrum $\widetilde{S}(\mathbf{k}_\parallel)$ in one case and a real $\widetilde{S}(\mathbf{k}_\parallel)$ measured by AFM or SNOM in the other case, we find that the intensity ACF is stretched in the direction parallel to the incident field. Then, the experimental anisotropic behavior is retrieved in both cases. In the incident polarization direction, the surface waves scattered from the surface diffusers are more coupled to each other, leading to a longer correlation length in this direction. In the transverse direction, the oscillations do not appear by using an ideal Gaussian-like surface ACF in the simulation. These subwavelength modulations are associated with the real surface height distribution and may be due to the random and disordered character of the structure pattern.

On the other hand, in the model used for the simulation, a rough but homogeneous medium is considered. The inhomogeneity of the random gold films cannot be taken into account. This might explain the numerical discrepancy between simulations and experimental values. Moreover, the finite size of the tip aperture that collects the scattered light has not been taken into account.

B. Intensity autocorrelation function evolution as a function of the observation distance z

We have performed several simulations of the intensity ACF for different observation distances z. For each graph,

(a)

(b)
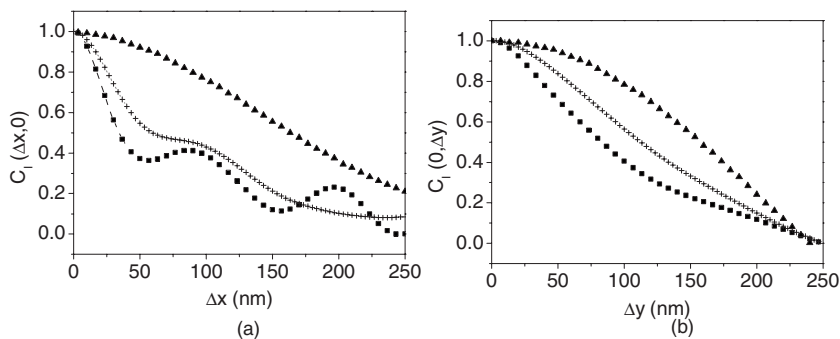
FIG. 9. The correlation curves are plotted (a) in the perpendicular direction to the incident field $C_I(\Delta x, y=0)$ and (b) in the parallel direction to the incident field $C_I(x=0, \Delta y)$. The graphs are plotted for $z=1$ nm (■), $z=10$ nm (+), and $z=100$ nm (▲).
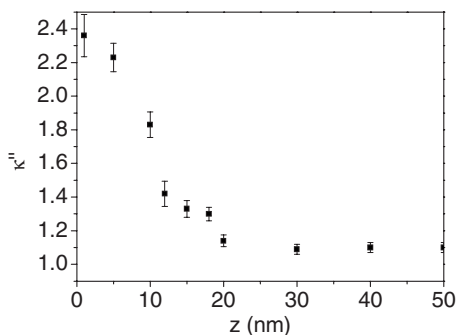
FIG. 10. Anisotropic factor κ as a function of the observation distance z.

the correlation function was calculated from the intensity distribution obtained from Eq. (4). For each simulation, we have introduced in Eq. (4) the Fourier transform $\widetilde{S}(\mathbf{k}_{\parallel})$ of the measured surface profile $S(x,y)$. In Fig. 9, the correlation functions are plotted for three observation distances (1, 10, and 100 nm).

As the observation distance z is increasing, the subwavelength oscillations are smoothed and tend to completely disappear in the far field. Besides, the anisotropic behavior vanishes accounting for the evolution from near-field speckle to the classical far-field speckle.

To point out the transition from the near-field to the far-field regime, the anisotropy factor κ'' is calculated and is plotted versus z in Fig. 10.

The anisotropy factor is, without surprise, continuously decreasing with z increasing. We note that the optical intensity ACF remains anisotropic for distances $z < 20$ nm and that it rapidly decreases from $z = 1$ nm to $z = 11$ nm. We can notice that the anisotropic factor values close to the experimentally determined one ($\kappa \simeq 1.5$) lead to theoretical distances z between 10 and 15 nm which are in good agreement

with the typical tip-to-sample distance expected in the experiment. So, for the conclusion of this section, we can underline that the model used[9] is relevant to describe the anisotropic behavior of the near-field speckle and its evolution to the far-field regime. The near-field speckle oscillations are also described by this model but, to give prominence to these oscillations, it has been necessary to input a nonrealistic z value ($z = 1$ nm) in the model. As previously mentioned, this numerical discrepancy may be due to the fact that the considered medium is rough but homogeneous.

V. CONCLUSION

In summary, the intensity scattered from random metallic films was studied in the near-field zone both in experimental and numerical ways. The intensity distribution, measured using an aperture SNOM, is statistically analyzed with the ACF. The results display two main characteristics of the near-field speckle: an anisotropic intensity ACF with a stronger coupling of the evanescent waves in the polarization direction; in the transverse direction, subwavelength oscillations associated with the specific topographic distribution. These behaviors have been completely retrieved with a simulation of near-field intensity taking account of the real surface. These results provide the experimental evidence of the strong polarization dependence of the near-field speckle. It could be usefully extended to more complex regimes including plasmon resonances on metallic films.

ACKNOWLEDGMENTS

*Present address: Laboratoire Aimé Cotton (UPR CNRS 3321), Bâtiment 505, 91405 Orsay Cedex, France. julien.laverdant@lac.u-psud.fr

[1] R. Berkovits and S. Feng, Phys. Rep. **238**, 135 (1994).

[2] P. Sheng, *Introduction to Wave Scattering, Localization and Mesoscopic Phenomena* (Academic, New York, 1995).

[3] M. C. van Rossum and T. M. Nieuwenhuizen, Rev. Mod. Phys. **71**, 313 (1999).

[4] A. R. McGurn and A. A. Maradudin, Phys. Rev. B **39**, 13160 (1989).

[5] B. Shapiro, Phys. Rev. Lett. **57**, 2168 (1986).

[6] I. Freund and D. Eliyahu, Phys. Rev. A **45**, 6133 (1992).

[7] J. Uozomi, M. Ibrahim, and T. Asakura, Opt. Commun. **156**, 350 (1998).

[8] J. W. Goodman, *Statistical Optics* (Wiley, New York, 2000).

[9] J.-J. Greffet and R. Carminati, Ultramicroscopy **61**, 43 (1995).

[10] V. Emiliani, F. Intonti, M. Cazayous, D. S. Wiersma, M. Colocci, F. Aliev, and A. Lagendijk, Phys. Rev. Lett. **90**, 250801 (2003).

[11] A. Apostol and A. Dogariu, Phys. Rev. Lett. **91**, 093901 (2003).

[12] C. Liu and S.-H. Park, Opt. Lett. **30**, 1602 (2005).

[13] G. Rasigni, F. Varnier, M. Rasigni, J.-P. Palmari, and A. Llebaria, Phys. Rev. B **25**, 2315 (1982).

[14] Y. Zhang and S. Sundararajan, Appl. Phys. Lett. **88**, 141903 (2006).

[15] H. Raether, *Surface Plasmons on Smooth and Rough Surfaces and on Grating* (Springer-Verlag, Berlin, 1988).

[16] A. K. Sarychev and V. M. Shalaev, Phys. Rep. **335**, 275 (2000).

[17] P. Gadenne, Y. Yagil, and G. Deutscher, J. Appl. Phys. **66**, 3019 (1989).

[18] D. Courjon and C. Bainier, Rep. Prog. Phys. **57**, 989 (1994).

[19] S. Buil, J. Aubineau, J. Laverdant, and X. Quélin, J. Appl. Phys. **100**, 063530 (2006).

[20] J. E. Sipe, J. Opt. Soc. Am. B **4**, 481 (1986).

[21] J.-J. Greffet and R. Carminati, Prog. Surf. Sci. **56**, 133 (1997).